Heavy ion charge-state distribution effects on energy loss in plasmas

Manuel D. Barriga-Carrasco*
E.T.S.I. Industriales, Universidad de Castilla-La Mancha, E-13071 Ciudad Real, Spain
(Received 23 July 2013; published 30 October 2013)

According to dielectric formalism, the energy loss of the heavy ion depends on its velocity and its charge density. Also, it depends on the target through its dielectric function; here the random phase approximation is used because it correctly describes fully ionized plasmas at any degeneracy. On the other hand, the Brandt-Kitagawa (BK) model is employed to depict the projectile charge space distribution, and the stripping criterion of Kreussler *et al*. is used to determine its mean charge state $\langle Q \rangle$. This latter criterion implies that the mean charge state depends on the electron density and temperature of the plasma. Also, the initial charge state of the heavy ion is crucial for calculating $\langle Q \rangle$ inside the plasma. Comparing our models and estimations with experimental data, a very good agreement is found. It is noticed that the energy loss in plasmas is higher than that in the same cold gas cases, confirming the well-known enhanced plasma stopping (EPS). In this case, EPS is only due to the increase in projectile effective charge Q_{eff}, which is obtained as the ratio between the energy loss of each heavy ion and that of the proton in the same plasma conditions. The ratio between the effective charges in plasmas and in cold gases is higher than 1, but it is not as high as thought in the past. Finally, another significant issue is that the calculated effective charge in plasmas Q_{eff} is greater than the mean charge state $\langle Q \rangle$, which is due to the incorporation of the BK charge distribution. When estimations are performed without this distribution, they do not fit well with experimental data.

DOI: 10.1103/PhysRevE.88.043107 PACS number(s): 52.40.Mj, 52.58.Hm, 52.20.Hv, 52.25.Mq

I. INTRODUCTION

In recent decades, energy loss of ions in matter has been the subject of research. Specifically, energy loss in solids and gases has been studied for almost a century; therefore, there are numerous models that adequately reproduce and explain the experimental data [1–5]. However, the interaction of charged particles with fully ionized matter (plasma) is still not completely understood, and there are only few experimental data that support the development of theories on this subject [6–13].

The energy loss of ions in plasmas is relevant for many applications in different fields of science, such as heavy ion inertial fusion [14], the use of plasma targets as focusing [6,15,16] or stripping devices [9,17,18] of heavy ion beams, the transverse cooling of an intense ion beam by a magnetized electron beam [19], and the investigation of warm dense matter [20]. Therefore, many laboratories continue with experiments on the interaction of ion beams with ionized matter [21–26]. The electronic stopping of projectiles in plasmas differs from the stopping in solids and gases, owing to the properties of plasma. In this last case, a projectile interacts not only with neutral atoms, but also with the ions and free electrons in the target.

An important aspect when calculating the electronic stopping of ions is to know the projectile charge state. There are various processes that modify the projectile charge state when it travels through the target (electron capture or loss). As it is not possible to measure this parameter for any projectile and at any position during its travel, it must be determined theoretically.

The charge state of the projectile increases when passing through a target (projectile loses electrons) principally by collisions with target ions, but it also decreases due to the capture of the electrons bound to ions (recombination). There are other effects that change the charge state of the projectile, but these are the two dominant mechanisms.

In the case where a projectile traverses a solid, a kind of equilibrium charge state is reached after it travels a short distance through the target. This equilibrium charge state is primarily a function of velocity and the initial charge state before entering the target [4,27–30].

The charge state of projectiles passing through fully ionized plasmas was first studied by Nardi and Zinamon [3] who showed theoretically that the charge state is significantly higher than when the same projectiles pass through solids. Later, this effect was verified experimentally [12,31–34].

This increase in the ion charge state traveling through completely ionized plasma is mainly due to the reduction in the recombination processes of the projectile. This is because of the smaller number of bound electrons in plasmas, which are captured by the projectile in the case of a solid or a partially ionized gas (direct free electron capture from a moving projectile violates the simultaneous conservation of energy and momentum). The charge state enhancement affects the value of the energy deposited in the target significantly, resulting in an increase in electronic stopping in plasmas compared with cold matter.

Experiments reported in the literature [6,12,31,33] show that the electronic stopping of ions in plasmas is higher than the electronic stopping in cold matter for two main reasons: the increase in projectile charge state mentioned above, and the more efficient energy transfer with the free electrons of the plasma than with the bound electrons of the solid. In this paper, we focus on analyzing the first reason for the increase in electronic stopping, the projectile charge state enhancement. This study is based on the dielectric formalism to analyze the charge distribution and the charge state of the

*manueld.barriga@uclm.es

projectile. To distinguish the enhanced stopping due to the higher number of free electrons in plasmas compared with cold matter, we use only fully ionized plasmas or electron gases as the targets.

II. DIELECTRIC FORMALISM

Many models have been developed to calculate projectile energy losses due to electronic stopping in different targets. One that is used most widely is the dielectric formalism introduced by Fermi [35] and developed by Fermi and Teller [36].

In the dielectric formalism, the electron response, in an isotropic and homogeneous material, to a perturbation produced by an external charge density $\rho_{\rm ext}(\boldsymbol{r},t)$ is contained in the dielectric function $\epsilon(\boldsymbol{r},t)$ of the medium.

In the phase space, the first Maxwell equation relates the displacement vector $\boldsymbol{D}(\boldsymbol{k},w)=\epsilon(\boldsymbol{k},w)\,\boldsymbol{E}(\boldsymbol{k},w)$ with the external charge density $\rho_{\rm ext}(\boldsymbol{r},t)$,

$$\nabla \boldsymbol{D}(\boldsymbol{k},w)=4\pi\rho_{\rm ext}(\boldsymbol{k},w),$$

in Gaussian units. Moreover, the electric field and total potential $\phi_{\rm tot}$ are related by the expression,

$$\boldsymbol{E}(\boldsymbol{k},w)=-i\,\boldsymbol{k}\phi_{\rm tot}(\boldsymbol{k},w).$$

Therefore, the total potential is obtained in terms of the external charge density,

$$\phi_{\rm tot}(\boldsymbol{k},w)=\frac{4\pi\rho_{\rm ext}(\boldsymbol{k},w)}{k^2\epsilon(\boldsymbol{k},w)}. \tag{1}$$

If the projectile is atomic in nature, the external charge density $\rho_{\rm ext}(\boldsymbol{r},t)$ will consist of a nucleus with charge Z, presumably pointlike, and an electron cloud with a charge density $\rho_e(\boldsymbol{r},t)$ that will move with velocity $\boldsymbol{v}$, provided that the relative velocity between the nucleus and the electron cloud is negligible. Thus, this is written as

$$\rho_{\rm ext}(\boldsymbol{r},t)=Z\delta(\boldsymbol{r}-\boldsymbol{v}t)-\rho_e(\boldsymbol{r}-\boldsymbol{v}t),$$

whose Fourier transform is

$$\rho_{\rm ext}(\boldsymbol{k},w)=2\pi\delta(w-\boldsymbol{k}\cdot\boldsymbol{v})[Z-\rho_e(\boldsymbol{k})], \tag{2}$$

where $\rho_e(\boldsymbol{k})$ is the Fourier transform of the electron density of the projectile in absolute value because the minus sign in the equations above indicates the negative value of the electron charge.

Substituting this expression into Eq. (1), the following relationship between the total potential and the external charge density is achieved:

$$\phi_{\rm tot}(\boldsymbol{k},w)=8\pi^2\delta(w-\boldsymbol{k}\cdot v)\frac{Z-\rho_e(\boldsymbol{k})}{k^2\epsilon(\boldsymbol{k},w)}.$$

The induced potential can be obtained by subtracting the Colombian potential [where $\epsilon(\boldsymbol{k},w)=1$ in Gaussian units] from the total potential,

$$\phi_{\rm ind}(\boldsymbol{k},w)=8\pi^2\delta(w-\boldsymbol{k}\cdot\boldsymbol{v})\frac{Z-\rho_e(\boldsymbol{k})}{k^2}\left[\frac{1}{\epsilon(\boldsymbol{k},w)}-1\right]. \tag{3}$$

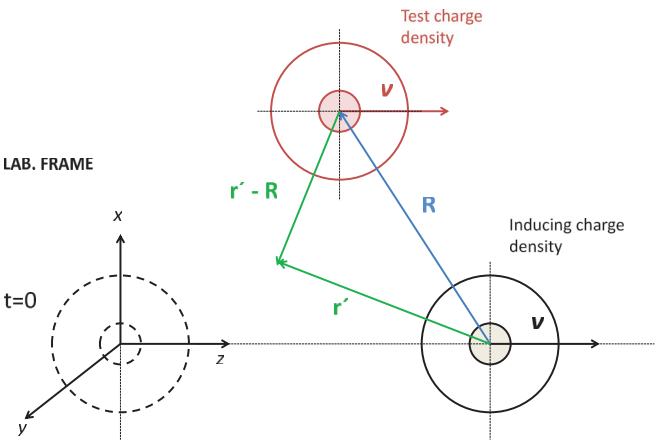

FIG. 1. (Color online) Inducing and test charge density traveling through a plasma with velocity $\boldsymbol{v}$. Dashed lines: position of inducing charge density at time $t=0$ and solid lines: position of inducing and test charge density at time t.

Then, the potential energy due to the induced potential acting on a test charge density $\rho'_{\rm ext}$ can be calculated as

$$U(\boldsymbol{R},t)=\int dr'\phi_{\rm ind}(\boldsymbol{r}',t)\rho'_{\rm ext}(\boldsymbol{r}'-\boldsymbol{R},t),$$

where $\boldsymbol{R}$ is the vector position of $\rho'_{\rm ext}$ with respect to the position of the inducing charge density (see Fig. 1).

Rewriting this equation in terms of the Fourier transforms, we get

$$U(\boldsymbol{R},t)=\frac{1}{(2\pi)^8}\int d\boldsymbol{r}'\int d\boldsymbol{k}\int dw\;\phi_{\rm ind}(\boldsymbol{k},w)\,e^{i(k\cdot r'-wt)}\times\int d\boldsymbol{k}'\int dw'\rho'_{\rm ext}(\boldsymbol{k}',w')e^{i(\boldsymbol{k}'\cdot r'-w't)}e^{-i\boldsymbol{k}'\cdot\boldsymbol{R}}.$$

Then, employing Eqs. (2) and (3) for the external charge density and the induced potential, respectively, and considering $\rho'_{\rm ext}=Z'-\rho'_e(k)$,

$$U(\boldsymbol{R},t)=\frac{1}{2\pi^2}\int d\boldsymbol{k}\frac{[Z-\rho_e(\boldsymbol{k})][Z'-\rho'_e(\boldsymbol{k})]}{k^2}\times\int dw\;e^{i\boldsymbol{k}\cdot R}\delta(w-\boldsymbol{k}\;\cdot\;\boldsymbol{v})\left[\frac{1}{\epsilon(\boldsymbol{k},w)}-1\right].$$

After this, vectors $\boldsymbol{r}$ and $\boldsymbol{k}$ are divided into a component perpendicular to the velocity of the projectile and into another parallel to it, i.e., $\boldsymbol{r}\equiv(\boldsymbol{r}_\perp,\boldsymbol{r}_)$ and $\boldsymbol{k}\equiv(\boldsymbol{k}_\perp,\boldsymbol{k}_)$. Also, vector $d\boldsymbol{k}$ is separated into cylindrical coordinates, and we make a variable change $k=\sqrt{k_\perp^2+w^2/v^2}$, which sets the limit integration over w, $kv\geqslant w$, and as $k_\perp$ is real, we obtain

$$U(\boldsymbol{R},t)=\frac{2}{\pi v}\int_0^\infty d\boldsymbol{k}\frac{[Z-\rho_e(k)][Z'-\rho'_e(k)]}{k}\times\int_0^{kv}dw\;J_0(R_\perp\sqrt{k^2-w^2/v^2})\times\left\{\cos\left(\frac{wR_\parallel}{v}\right)\mathrm{Re}\left[\frac{1}{\epsilon(\boldsymbol{k},w)}-1\right]-\sin\left(\frac{wR_\parallel}{v}\right)\mathrm{Im}\left[\frac{1}{\epsilon(\boldsymbol{k},w)}\right]\right\},$$

where J_0 is the Bessel function of the zeroth order. In a first approximation, we assume that the electron densities have spherical symmetry so that we can replace the vector dependence of the electron densities $\rho_e(\boldsymbol{k})$ by linear dependence $\rho_e(k)$.

Force components in directions parallel and perpendicular to the projectile velocity vector are achieved by obtaining the gradient of the potential energy,

$$F_{\parallel}(R_{,}R_{\perp}) = \frac{2}{\pi v}\int_0^{\infty} d\boldsymbol{k}\frac{[Z-\rho_e(k)]\,[Z'-\rho'_e(k)]}{k}\int_0^{kv} dw\; w J_0(R_{\perp}\sqrt{k^2-w^2/v^2})$$
$$\times\left\{\sin\left(\frac{wR_{\parallel}}{v}\right)\mathrm{Re}\left[\frac{1}{\epsilon(\boldsymbol{k},w)}-1\right]+\cos\left(\frac{wR_{\parallel}}{v}\right)\mathrm{Im}\left[\frac{1}{\epsilon(\boldsymbol{k},w)}\right]\right\},$$
$$F_{\perp}(R_{,}R_{\perp}) = \frac{2}{\pi v}\int_0^{\infty} d\boldsymbol{k}\frac{[Z-\rho_e(k)][Z'-\rho'_e(k)]}{k}\int_0^{kv} dw\sqrt{k^2-w^2/v^2}$$
$$\times J_1(R_{\perp}\sqrt{k^2-w^2/v^2})\left\{\cos\left(\frac{wR_{\parallel}}{v}\right)\mathrm{Re}\left[\frac{1}{\epsilon(\boldsymbol{k},w)}-1\right]-\sin\left(\frac{wR_{\parallel}}{v}\right)\mathrm{Im}\left[\frac{1}{\epsilon(\boldsymbol{k},w)}\right]\right\},$$

where J_1 is the Bessel function of the first order. It is important to show that the force components do not depend explicitly on time.

The force that acts on the projectile itself $R_{=}R_{\perp}=0$ has no perpendicular part $F_{\perp}=0$, i.e., it has only a parallel part,

$$F_{=}\frac{-2}{\pi v^2}\int_0^{\infty} d\boldsymbol{k}\frac{[Z-\rho_e(k)]^2}{k}\int_0^{kv} dw\; w\;\mathrm{Im}\left[\frac{-1}{\epsilon(\boldsymbol{k},w)}\right],$$

the direction of which is opposite to the projectile velocity, implying that it will stop or will lose its energy through the target. If the projectile travels in the z direction, the energy loss will be $dE=-F_d z$, and then the electronic stopping can be expressed as

$$S_p(v)=\frac{dE}{dz}=-F_{=}\frac{2}{\pi v^2}\int_0^{\infty} d\boldsymbol{k}\frac{[Z-\rho_e(k)]^2}{k}$$
$$\times\int_0^{kv} dw\; w\;\mathrm{Im}\left[\frac{-1}{\epsilon(\boldsymbol{k},w)}\right]. \qquad (4)$$

According to this expression, the electronic stopping of the projectile depends on its velocity and the square of the Fourier transform of its charge density $Z-\rho_e(k)$; however, it depends on the target through the energy loss function $\mathrm{Im}(1/\epsilon)$. Then, to be able to calculate the electronic stopping of the projectile, it is necessary to define its electron distribution $\rho_e(k)$ and to characterize the target material by its dielectric function $\epsilon(\boldsymbol{k},w)$.

III. TARGET DESCRIPTION

The dielectric function of an electron gas without damping, i.e., without considering collisions between its electrons, was calculated first by Lindhard [37] in the random phase approximation (RPA). The RPA usually is valid when these electron collisions are not significant in the gas [38]. However, in this paper, we will study all kinds of electron gases, and therefore, these collisions have to be taken into account.

Mermin [39] derived an expression for the dielectric function considering plasma electron collisions but only preserving the local particle density. This function has successfully been applied to solids (dense degenerate electron gases) [40], to classical plasmas (nondegenerate electron gases) [41], and to partially degenerate plasmas [42]. For solids, the Mermin dielectric function (DF) was used, obtaining the electron collision frequency from experiments [43,44], but for plasmas, this frequency must be calculated *a priori*. Many papers have been devoted to calculating this frequency [45–47], whereas, others treat it as a free parameter [48,49]. In the present investigation, these values are taken from a previous calculation [50].

Recently, a new DF has been calculated that includes electron collisions but preserves the three conservation laws (density, momentum, and energy) for plasmas at any degeneracy [51,52]. This full conserving dielectric function reproduces the former RPA DF and Mermin DF. Differences in calculations of energy loss between the full conserving dielectric function and the RPA DF were found to be a maximum of 2% for plasmas with very high collision frequencies [53]. This means that collisions are not important for energy loss calculations. Therefore, for this paper, we will use the simpler RPA DF to calculate electronic stopping.

RPA DFs can be developed in terms of the wave number k and of the frequency ω provided by a consistent quantum mechanical analysis [using atomic units (a.u.), $e=\hbar=m_e=1$, to simplify the formulas],

$$\epsilon_{\mathrm{RPA}}(\boldsymbol{k},w)=1+\frac{1}{\pi^2 k^2}\int d^3k'\frac{f(\boldsymbol{k}+\boldsymbol{k}')-f(\boldsymbol{k}')}{w+i\nu-(E_{k+k'}-E_{k'})}, \qquad (5)$$

where $E_{\boldsymbol{k}}=k^2/2$. The temperature dependence is included through the Fermi-Dirac function,

$$f(\boldsymbol{k})=\frac{1}{1+\exp[\beta(E_k-\mu)]}, \qquad (6)$$

where $\beta=1/k_BT$ and μ is the chemical potential of the plasma with electron density n_e and temperature T. In this part of the analysis, we assume the absence of collisions such that the collision frequency tends to zero $\nu\to 0$.

Analytic RPA DFs for plasmas at any degeneracy can be obtained directly from Eq. (5) [54,55],

$$\epsilon_{\mathrm{RPA}}(\boldsymbol{k},w)=1+\frac{1}{4z^3\pi\, k_F}[g(u+z)-g(u-z)], \qquad (7)$$

where $g(x)$ corresponds to

$$g(x) = \int_0^\infty \frac{y\, dy}{\exp(Dy^2 - \beta\mu) + 1} \ln\left(\frac{x+y}{x-y}\right),$$

where $u = w/kv_F$ and $z = k/2k_F$ are the common dimensionless variables [37], $D = E_F\beta$ is the degeneracy parameter, and $v_F = k_F = \sqrt{2E_F}$ is the Fermi velocity in a.u.

IV. PROJECTILE DESCRIPTION

Describing the projectile involves determining how its charge density is distributed in space when traveling through a target. This requires knowing the number of electrons bound to the nucleus of the projectile, which changes while traveling due to electron capture and loss processes. The Brandt-Kitagawa (BK) model is used to describe the projectile space distribution.

In the BK model [56], the density of electrons bound to the projectile is established by a generic orbital that depends on variational parameter Λ,

$$\rho_{e,\mathrm{BK}}(r) = \frac{N}{4\pi\Lambda^3}\frac{\Lambda}{r}e^{-r/\Lambda}, \tag{8}$$

where N is the number of electrons bound to the projectile, r is the distance to the nucleus, and Λ fulfills

$$\frac{1}{\Lambda} = \frac{1}{N}\int \frac{\rho_e(r)}{r} dr.$$

Integrating the electron density over all orientations in space, the probability $P(r)$ that an electron was in a spherical shell of thickness dr at a distance r from the nucleus is obtained

$$P(r) = \int_0^{2\pi} d\Phi \int_{-1}^{1} d(\cos\theta)\, r^2\rho_e(r) = 4\pi r^2\rho_e(r)\, dr,$$

where $4\pi r^2\rho_e(r)$ is the radial distribution function. Meanwhile, as Λ increases, the radial distribution function extends to the space.

According to the work of Brandt-Kitagawa [56], the internal energy of the projectile can be written as the sum of the potential energy of the nucleus electron E_{ne} and electron-electron E_{ee} interactions and the kinetic energy of the electrons E_c,

$$E = E_{ne} + \lambda E_{ee} + E_c,$$

where λ is another variational parameter that introduces corrections due to not considering the correlation and interchange energy contributions in the electron-electron interaction potential,

$$\begin{aligned} E_{ne} &= -Z\int dr \frac{\rho_e(r)}{r} = -\frac{ZN}{\Lambda}, \\ E_{ee} &= \frac{1}{2}\int d\boldsymbol{r}\int d\boldsymbol{r}' \frac{\rho_e(r)\,\rho_e(r')}{|\boldsymbol{r}-\boldsymbol{r}'|} = \frac{N^2}{2\Lambda} \\ &= -\frac{1}{2}\left(\frac{3}{4}\pi\right)^{2/3}\left(\frac{3}{5}\right)^{5/3}\Gamma\left(\frac{4}{3}\right)\frac{N^{5/3}}{\Lambda^2} = 0.24\frac{N^{5/3}}{\Lambda^2}, \end{aligned}$$

where Γ is the γ function.

Imposing the condition $\frac{\partial E}{\partial \Lambda} = 0$ in order to set the Λ value for which the internal energy of the projectile is minimized, we get

$$\Lambda(Z,N) = \frac{0.48N^{2/3}}{Z - \frac{\lambda}{2}N}. \tag{9}$$

To determine the value of the λ parameter, it is assumed that the more stable chemical species is the one that has the same number of electrons bound to the nucleus as the number of protons,

$$\left.\frac{\partial E}{\partial N}\right|_{N=Z} = 0.$$

Thus, using Eq. (9) leads to the value of $\lambda = 2/7$.

The Λ parameter value increases with the number of electrons bound to the projectile. Moreover, with the increasing atomic number of the projectile Z, the value of Λ for $N = Z$ is lower because a greater nuclear charge leads to compaction of the radial distribution function $P(r)$ associated with electrons.

Finally, the Fourier transform of the electron density needed in Eq. (8) is

$$\rho_{e,\mathrm{BK}}(k) = \frac{N}{1 + (k\Lambda)^2}. \tag{10}$$

Observing Eq. (10), we see that increasing parameter Λ decreases the Fourier transform of the electron density, i.e., the extension of the orbital will be larger. This means that as parameter Λ increases, the projectile charge "seen" by the electrons of the target $(Z - \rho_e)$ will be greater. In fact, if it is verified that $\Lambda \to \infty$, the projectile would behave like a point charge Z completely stripped of electrons. As variational parameter Λ increases, the charge density of the projectile becomes greater, regardless of momentum transferred (k), and therefore, electronic stopping will also be higher [see Eq. (4)].

Another observation we can make is that $(Z - \rho_e)$ tends to Z with increasing momentum transferred, and if the latter becomes small, $(Z - \rho_e)$ vanishes. Thus, when target electrons interact with a projectile charge near its nuclear value $(\rho_e \to 0)$, the momentum transferred will be higher, whereas, when interacting with a neutral projectile, the momentum transferred will be zero. As the projectile charge increases, the variational parameter Λ decreases (charge is more compact), increasing its electron density (see Fig. 2).

V. PROJECTILE CHARGE

When a projectile is heavy, its charge state can be very diverse with corresponding complexity in any calculation that depends on it. Hence, most authors use a mean charge state when calculating electronic stopping.

One of the procedures used to determine the mean charge state of a heavy projectile is based on the stripping criterion of Bohr [27], whereby the bound electrons of the projectile will be ionized; the ones whose relative velocity to the nucleus is less than the velocity of the nucleus to the target. This implies that the mean charge depends on the atomic number and on the velocity of the projectile.

Kreussler *et al.* [29] suggested that the mean charge state of the projectile $\langle Q\rangle$ not only depends on the relative velocity of the latter to the target, but also on the relative velocity between the projectile (v) and the electrons of the target (v_e),

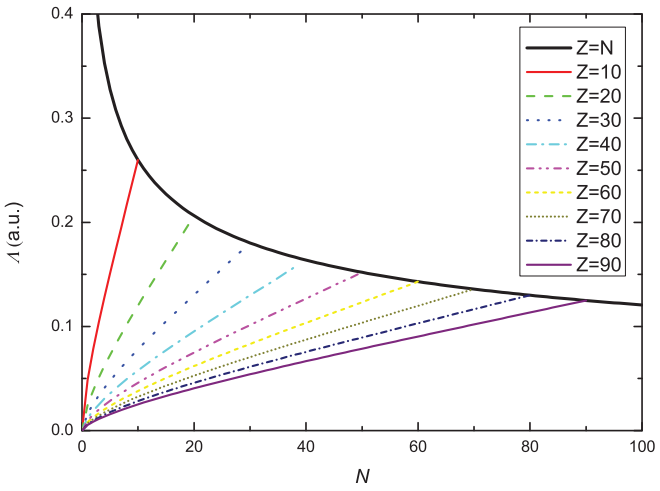

FIG. 2. (Color online) Λ, Eq. (9), as a function of N, number of electrons bound to the nucleus for different projectiles. Solid line corresponds to the curve $N = Z$.

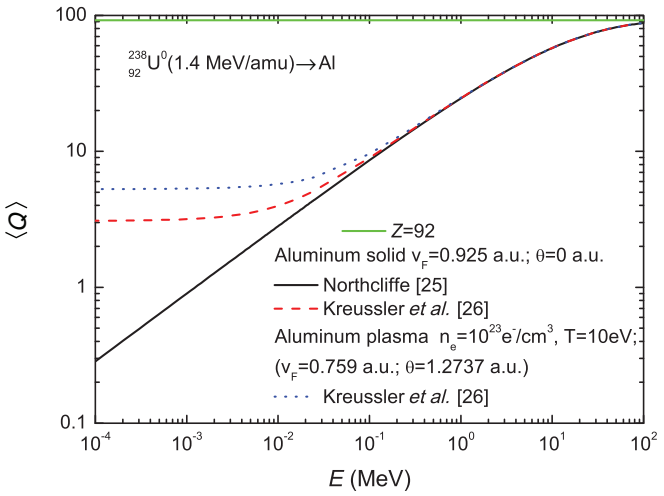

FIG. 3. (Color online) Mean charge state of uranium ($Z = 92$) traveling through an aluminum solid or plasma ($n_e = 10^{23} e^-/\text{cm}^2$; $T = 10$ eV) as a function of its velocity when using the model of Kreussler *et al.* [29], Eq. (14), or the Northcliffe model (not depending on target material $v_r = v$) [28].

i.e., $v_r = |\boldsymbol{v} - \boldsymbol{v}_e|$. Considering all the possible orientations of vector $\boldsymbol{v} - \boldsymbol{v}_e$ gives

$$v_r = |\boldsymbol{v} - \boldsymbol{v}_e| = \frac{v_e^2}{6v}\left[\left(\frac{v}{v_e}+1\right)^3 - \left|\frac{v}{v_e}-1\right|^3\right]. \quad (11)$$

Their studies were on solid materials and, therefore, for electron velocity, only the valence electrons of the target are considered, i.e., only its Fermi velocity is considered. Averaging over the Fermi sphere $0 \leqslant v_e \leqslant v_F$, we get

$$v_r = \frac{v_F^2}{10v}\left\{\left(\frac{v}{v_F}+1\right)^3 - \left|\frac{v}{v_F}-1\right|^3 + 4\left(\frac{v}{v_F}\right)^2 + H\left(\frac{v_F}{v}-1\right)\left[\frac{3v}{2v_F} - 4\left(\frac{v}{v_F}\right)^2 + 3\left(\frac{v}{v_F}\right)^3 - \frac{1}{2}\left(\frac{v}{v_F}\right)^5\right]\right\}, \quad (12)$$

where $H(\cdots)$ is the Heaviside step function.

In the case of plasma, the electron velocity is defined by its corresponding Fermi velocity, as solids, plus a term due to temperature,

$$v_e = \left(2 \times \tfrac{3}{5}E_F + 3k_BT\right)^{1/2} = \left(\tfrac{3}{5}v_F^2 + 3v_{\text{the}}^2\right)^{1/2} = \left(\tfrac{3}{5}\right)^{1/2} v_F\left(1 + \tfrac{5}{2}\theta\right)^{1/2}, \quad (13)$$

where T is the plasma temperature, $v_{\text{the}} = \sqrt{k_BT}$ is the thermal velocity, k_B is the Boltzmann constant, $\theta = \frac{k_BT}{E_F} = \frac{2v_{\text{the}}^2}{v_F^2}$ is the reduced plasma temperature, and v_F is the Fermi velocity $E_F = \frac{1}{2}v_F^2$ in a.u. By substituting this expression into Eq. (11), the relative velocity between the projectile and the plasma electrons is obtained.

The mean charge state is then calculated as

$$\langle Q\rangle = Z - \langle N\rangle = Z - Ze^{-v_r/Z^{2/3}v_0}, \quad (14)$$

where Z is the projectile atomic number, $\langle N\rangle$ is the average number of bound electrons, and $Z^{2/3}v_0$ is the electron velocity bound to the projectile in the Thomas Fermi model in a.u. The mean charge state of the projectile increases at the same time as its relative velocity does, until it achieves the limit value $\langle Q\rangle = Z$ when the velocity is high enough.

Figure 3 shows the dependence of the mean charge state of a uranium projectile ($Z = 92$) with velocity when traversing an aluminum solid or plasma. The differences between them are significant at low energies; the mean charge state of the projectile is higher when it travels through the plasma because the relative velocity in the plasma includes the thermal velocity of the electrons [see Eq. (13)].

In Figs. 4(a) and 4(b), the influence of the plasma properties on the mean charge state of a uranium projectile is shown. We note that, when the plasma temperature or the plasma electron density increases, the mean charge state of the projectile also increases, i.e., the number of electrons bound to the projectile is smaller; this effect is more significant at low energies. This is because an increase in the plasma temperature or the plasma electron density implies a velocity augmentation of the target electrons [Eq. (13)] and, thus, a reduction in the relative velocity [Eq. (12)]. This effect is much more pronounced in the case of increasing plasma temperature. Looking at Fig. 4(a), we see that, for $T = 1000$ eV, the initial mean charge state is practically ten times that for $T = 10$ eV and half of the asymptotic value at high energies ($Z = 92$).

If initially, instead of throwing neutral projectiles, a charged particle is thrown, the ionization degree of Kreussler *et al.* [29] must be changed. In this case, the electrons bound to the nucleus of the projectile are defined by the following expression:

$$\langle N\rangle = N_0 e^{-v_r/Z^{2/3}v_0}, \quad (15)$$

where $N_0 = (Z - Q_0)$ means the initial electrons bound to the projectile nucleus and Q_0 is the initial charge state.

After obtaining the projectile mean charge state or the number of electrons bound to the projectile $\langle N\rangle$, we must include it in the former model describing the electron charge density to calculate the electronic stopping.

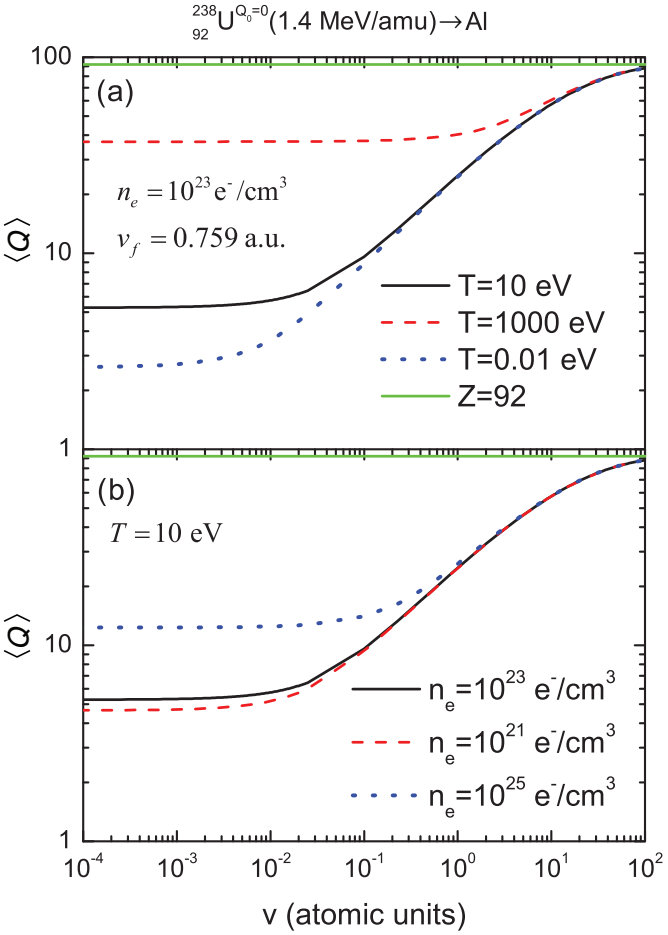

FIG. 4. (Color online) Mean charge state using the model of Kreussler *et al.* [29] and Eq. (14) of a uranium projectile ($Z = 92$), traveling through plasmas as a function of its velocity. (a) $n_e = 10^{23} e^-/\text{cm}^3$ and different temperatures and (b) $T = 10$ eV and different electron densities.

To include the ionization degree in the BK model is very easy, the only change we need to make is to replace N in Eq. (4) by Eq. (15). In this case, the electronic stopping is calculated according to the following expression:

$$S_p(v) = \frac{2}{\pi v^2}\int_0^\infty \frac{dk}{k}\left[Z - \frac{\langle N\rangle}{1+(k\Lambda)^2}\right]^2 \times \int_0^{kv} dw\, w\, \text{Im}\left[\frac{-1}{\epsilon(k,w)}\right], \quad (16)$$

where

$$\Lambda(v) = \frac{0.48\,\langle N\rangle^{2/3}}{Z - \frac{1}{7}\langle N\rangle}.$$

Figure 5 shows the electronic stopping using the BK model for various uranium charge states and one with the mean charge state of Kreussler *et al.* [29] $\langle Q\rangle$ as a function of its velocity in a plasma target. If the charge state fractions of uranium for this plasma were known, we would know each contribution to the total stopping, and we could compare it with the curve obtained using the mean charge state.

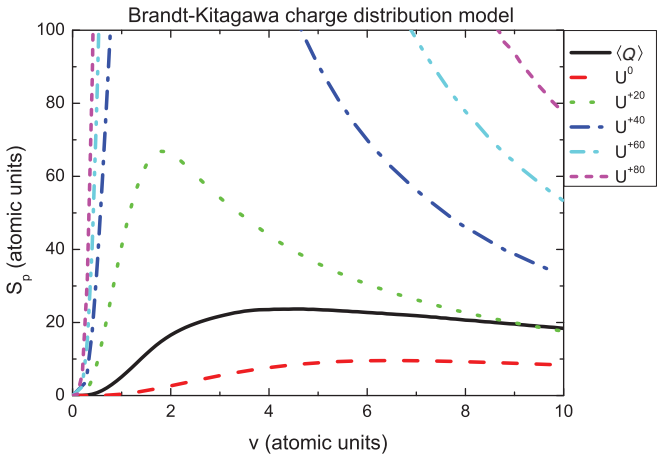

FIG. 5. (Color online) Electronic stopping of various uranium charge states and their mean charge state $\langle Q\rangle$ with $Q_0 = 0$, defined by the model of Kreussler *et al.* [29], see Eq. (14) as a function of its velocity in a plasma target with $n_e = 10^{23} e^-/\text{cm}^3$ and $T = 10$ eV using the Brandt-Kitagawa charge distribution model.

VI. COMPARISON WITH EXPERIMENTS

In this section, we compare the energy loss of atomic projectiles in fully ionized plasmas or electron gases, calculated from the models described above with experimental data from the literature. Many experiments are carried out in laboratories for measuring and calculating the charge state of ions passing through fully ionized matter [12,31,32,57]. Specifically, in this paper, we will reproduce the experiments performed at GSI (Darmstadt, Germany) by Weyrich *et al.* [31] and Hoffmann *et al.* [8] because they were among the first.

These two papers present experimental data of the energy loss of heavy ions in fully ionized hydrogen plasma formed from a discharge tube. The plasma is created by discharging the energy stored in a capacitor bank into a volume of hydrogen gas, which thereby is fully ionized. The hydrogen gas is confined in a 36-cm long quartz tube with pierced electrodes at both ends. By knowing the free electron density n_e and the temperature T_e of the plasma, it is possible to determine the ionization degree and, therefore, by the Saha equation, the number of neutral atoms if the plasma is in TE or local thermal equilibrium. Perpendicular to the axis, along the diameter of the tube, the plasma is optically thin, and spectroscopic methods can be applied to determine the free electron density and the temperature. Figure 6 shows the development of the free electron density n_e and the temperature T_e, measured with the absorption method. The maximum density and temperature that coincide with the maximum energy loss are found to be $2.9 \times 10^{17} e^-/\text{cm}^2$ and 2.1 eV, respectively. With these results, we know that the ionization degree between 25 and 30 μs is about 95%. Therefore, the free electron density is approximately the same as the original particle density of hydrogen atoms.

In these experiments, different heavy ion species, ranging from Ca to U, were used at an energy of 1.4 MeV/u because, within this energy region, the expected energy loss should be greatest. The measurement of the energy loss was carried out with a time-of-flight method. This has the advantage that only a few parameters are needed to determine the change in energy

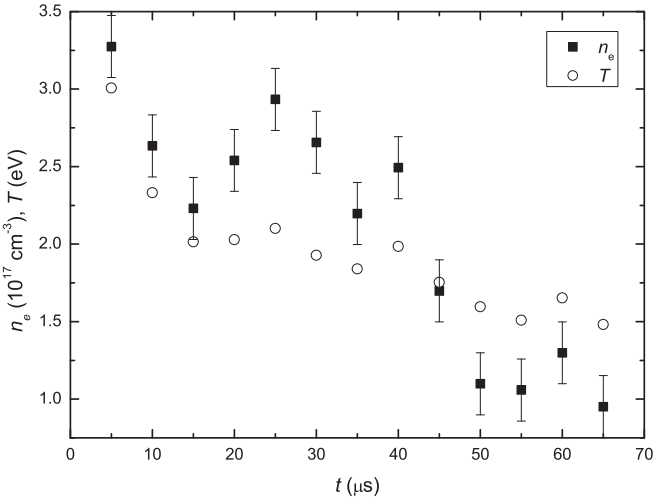

FIG. 6. Electron density and temperature as a function of plasma time development [8].

by the relation $\Delta E = 2(\Delta t/t_0)E_0$, where E_0 is the original ion energy of 1.4 MeV/u, t_0 is the vacuum time of flight of the ions on their flight path of 778 cm, and Δt is the measured increase in the flight time with hydrogen gas or plasma in the quartz tube.

The energy loss for four different ion species (^{40}Ca, ^{74}Ge, ^{84}Kr, and ^{238}U) was measured. Figure 7 shows the development of energy loss as a function of the plasma lifetime for ^{40}Ca, ^{84}Kr, and ^{238}U. The curve undergoes certain oscillations, and three maxima can be observed. The highest is between 25 and 30 μs after plasma ignition. By comparing Figs. 6 and 7, it can be seen that the oscillations in the energy loss are caused by similar oscillations in the electron density. This proves that the energy loss is a direct result of the free electron density of the plasma. Therefore, energy loss calculations will now be given as a function of the electron density. Additionally, Fig. 7 includes the theoretical calculations using our method explained in previous sections, specifically, the BK model with the mean charge state of Kreussler *et al.* [29]. As can be seen,

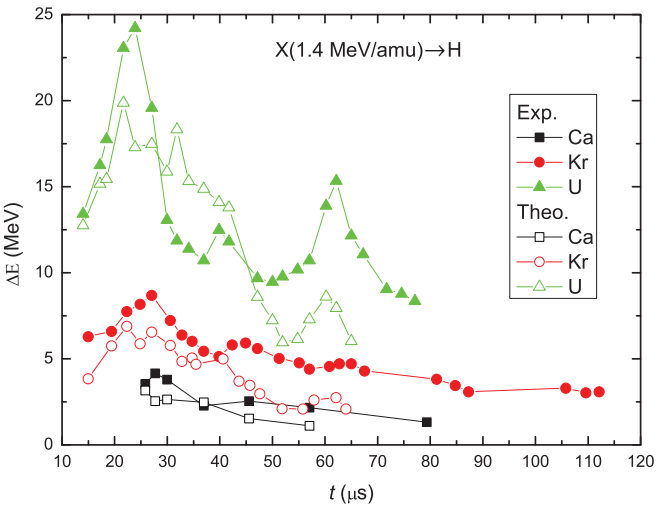

FIG. 7. (Color online) Energy loss of uranium, krypton, and calcium ions in hydrogen plasma.

the theoretical values are analogous to the experimental data, demonstrating a peaked structure, although not with exactly the same peak, which confirms our theoretical model.

The original Fig. 7 from Weyrich *et al.* [31] and Hoffmann *et al.* [8] compares their experimental results with the values for cold gas. It depicts a horizontal straight line for cold gases, but we disagree with this result because the energy loss in cold gases has to be measured with the same electron density and temperature values as for the plasmas. Nevertheless, it clearly illustrates the energy loss enhancement in plasmas. A correct comparison with cold gas will be shown in the following figures involving energy loss as a function of the electron density.

Figure 8 shows the energy loss experimental data together with our theoretical values for the former ions. The red circles denote the energy loss as a function of the free electron density as determined in the experiment for plasma. The black squares show the measured energy loss in the cold hydrogen gas of different electron densities. The blue triangles and green diamonds are our calculations. The blue triangles are estimated considering the initial charge state of all ions being equal to zero, $Q_0 = 0$, whereas, the green diamonds are equal to the initial charge state indicated in Hoffmann *et al.* [8]; $Q_0 = 13+$ for calcium, $Q_0 = 18+$ for germanium and for krypton, and $Q_0 = 33+$ for uranium. The initial charge state Q_0 is extremely relevant in establishing the mean charge state in equilibrium $\langle Q \rangle$ of the projectile during its transport through the plasma [Eq. (14)]. In the case of calcium, the mean charge state for an initial charge of $Q_0 = 0$ results in $\langle Q \rangle = 12.78+$, and for an initial charge of $Q_0 = 13+$, it results in $\langle Q \rangle = 17.47+$. Considering the figure, it appears that the estimation with $Q_0 = 0$ fits better to the experimental results. To check this, let us consider the next ion ^{74}Ge. In this case, the mean charge state for an initial charge state of $Q_0 = 0$ results in $\langle Q \rangle = 16.81+$, and for an initial charge of $Q_0 = 18+$, it results in $\langle Q \rangle = 25.35+$. Here, it is seen more clearly that the estimation with $Q_0 = 0$ fits better to the experimental values. As the atomic number of the projectile increases, the difference between the calculations with zero and nonzero initial charge states becomes more significant, fitting better the estimations with an initial charge near zero to the experimental data. Thus, it appears that the initial charges of Ca, Ge, Kr, and U projectiles are mostly neutral (minimally positive to be accelerated) before entering the plasma. This agrees with the results presented in Weyrich *et al.* [31] but not with those in Hoffmann *et al.* [8].

To better analyze the reason why there is a strong difference in Q_0 between our calculations and the results of Hoffmann *et al.* [8], we are going to try to reproduce their Fig. 7, presented in Ref. [8]. Thus, Fig. 9 represents the mean charge state of uranium as a function of its energy. The symbols are the calculations from Ref. [8], and the lines are our estimations for the different models: Northcliffe [28] and our model for different initial charge states $Q_0 = 0$ and $Q_0 = 33+$. The first thing to notice is that our mean charge state estimations depend strongly on the initial charge state. They do not converge until very high energies, far beyond the energy range studied in this paper. Our results for $Q_0 = 0$ are similar to the estimations for solids in Ref. [8], whereas, our results for $Q_0 = 33+$ are more similar to their results for plasma [8]. For

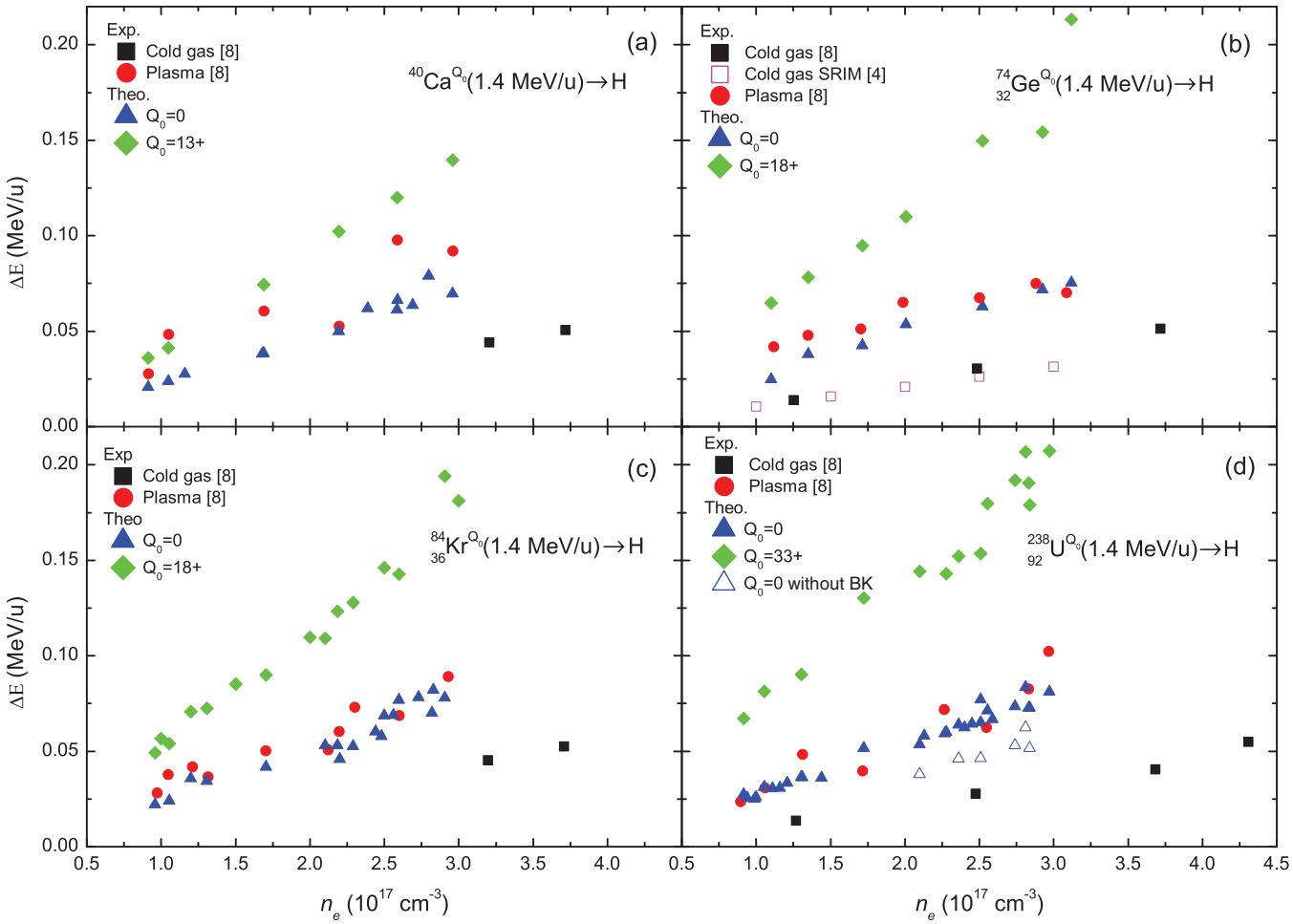

FIG. 8. (Color online) Experimental energy loss of several ions in a hydrogen plasma or cold gas as a function of their electron densities. Also, blue triangles are calculated considering the initial charge state of all ions equal to $Q_0 = 0$, whereas, the green diamonds show the initial charge state indicated in Hoffmann *et al*. [8].

$Q_0 = 33+$, their estimations declare that, at $E = 0$ MeV/u, the mean charge state is $\langle Q \rangle = 0$ [8], whereas, our model says

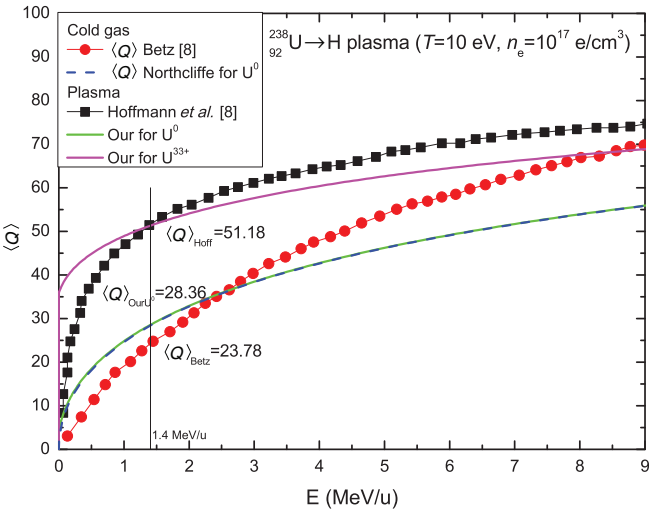

FIG. 9. (Color online) Mean charge state of uranium in a plasma as a function of its energy for different theoretical models.

$Q_0 = 33+$. A strange coincidence is that, for the experiment energy of 1.4 MeV/u, our result for $Q_0 = 33+$ intersects their computer model and gives the same value of $\langle Q \rangle = 51.18+$. However, as mentioned before, energy loss calculations using the initial charge state of 33+ do not fit well to the energy loss experimental data, and therefore, the idea of $Q_0 = 33+$ is abandoned.

Furthermore, in our results, there is only a small difference between the plasma and the cold gas case when using U^0. This means that, in our model, $\langle Q \rangle$ does not depend so much on temperature. It is noticed as well that the different models do not match for solids. The Betz estimation from Ref. [8] does not match our Northcliffe one, although the latter is similar to the SRIM data that are obtained from many experiments [4]. In Ref. [8], it is said that $\langle Q \rangle$ in solids is $28+$, which coincides with our estimation with the Northcliffe model but not with their Betz model, $23.78+$. Thus, we can conclude that the difference in the initial charge state between Ref. [8] and our results lies in their theoretical model to establish the initial charge state because our model fits very well with their experimental data.

Returning to Fig. 8, the experimental values for the cold gas cases are plotted as black squares [8]. The first thing that can be

TABLE I. Effective charge in plasma and cold gas for different projectiles.

Ion	Q_{eff} plasma	Q_{eff} cold gas	Ratio
$^{238}_{92}U^{0}$	34.43	24.26	1.42
$^{84}_{36}Kr^{0}$	19.79	16.98	1.17
$^{74}_{32}Ge^{0}$	18.40	14.92	1.23
$^{40}_{20}Ca^{0}$	13.39	12.14	1.10

TABLE II. Effective and mean charge states in plasmas for different projectiles.

Ion	Q_{eff} plasma	Q'_{eff}plasma	$\langle Q\rangle$ plasma
$^{238}_{92}U^{0}$	34.43	28.36	28.36
$^{84}_{36}Kr^{0}$	19.79	17.92	17.92
$^{74}_{32}Ge^{0}$	18.40	16.81	16.81
$^{40}_{20}Ca^{0}$	13.39	12.78	12.78

seen is that energy loss varies almost linearly with the electron density; it increases as the electron density does. Second, and more importantly, the energy loss for cold gas is lower than that for the hot plasma case, confirming the enhanced plasma stopping (EPS). Experimental data for cold gas from Ref. [8] are validated with the SRIM code [4] (pink open squares).

As mentioned in the Introduction, the EPS could be due to two main effects: the increase in projectile charge state or a more efficient energy transfer with the free electrons of the plasma. To discern the EPS due to the increase in charge state, it is convenient to compare the energy loss of each ion, not with the energy loss in cold gas, but with the energy loss of the proton in the same conditions, i.e., in the same plasma target. As the energy loss is proportional to the square of the effective charge, the ion effective charge traversing any material can be found as

$$Q_{\text{eff}} \equiv \sqrt{\Delta E_{\text{ion}}/\Delta E_{\text{prot}}}.$$

Thus, we can calculate the effective charges for each ion in plasma or in cold gas and compare them (see Table I). The Q_{eff} in plasmas is calculated from former figures for ions and from our theoretical model for protons, whereas, the Q_{eff} in cold gas also is obtained from figures for ions and the SRIM tables for protons [4]. As can be seen, the effective charge in plasma is higher than in the same cold gas, and this increase is due only to the increase in the projectile charge due to the plasma state of the target. In the Introduction, it is commented on that this enlargement is due mainly to the reduction in recombination processes of the projectile because of the smaller number of bound electrons in plasmas (more if these plasmas are fully ionized). In this paper, the reduction in the recombination process is taken into account through the relative velocity in the mean charge state estimation [Eq. (14)]. The factors for the enhancement range between 1.10 and 1.42. The heaviest ion, uranium, shows a slightly higher increase. This fact indicates that this effect is not as important as originally thought in the past.

Another thing that can be noticed is that the effective charge in plasmas Q_{eff} is greater than the mean charge states in plasmas $\langle Q\rangle$ (see Table II). This fact is directly due to the BK charge space distribution. It can be verified theoretically by performing energy loss calculations without the BK radial distribution in the energy loss estimation $\Delta E'_{\text{ion}}$ [see "$Q_0 = 0$ without BK" in Fig. 8(d)] and then calculating the new mean charge state as

$$Q'_{\text{eff}} \equiv \sqrt{\Delta E'_{\text{ion}}/\Delta E_{\text{prot}}}.$$

As expected, the results are the same when using Eq. (14). As our results with the BK charge distribution are closer to the experimental data, the use of the BK distribution is convenient.

VII. CONCLUSIONS

According to dielectric formalism, the energy loss of the heavy ion depends on its velocity and the square of the Fourier transform of its charge density. Also, it depends on the target through its energy loss function; in this paper, this is based on the RPA dielectric function that describes fully ionized plasmas superbly at any degeneracy.

The BK model is used to describe the projectile charge space distribution. The density of electrons bound to the projectile N is established by a generic orbital that depends on a variational parameter Λ, which, in turn, depends only on N and the nucleus charge Z. It is observed that, by increasing the parameter Λ, the extension of the orbital will become larger. Also, as the projectile charge increases, Λ decreases (charge is more compact), thereby, increasing its electron density.

Another model, this one to determine the mean charge state of a heavy projectile $\langle Q\rangle$, was based on the stripping criterion of Kreussler *et al.* [29], whereby the bound electrons of the projectile are ionized; the ones whose relative velocity to the nucleus is less than the relative velocity between the nucleus and the electrons of target. This implies that the mean charge depends on the electron density and temperature of the plasma. When the temperature or the electron density increases, the mean charge state of the projectile also increases. This effect is more significant at low projectile energies and higher plasma temperatures. The initial charge state of the heavy projectile has also been taken into account in this model because it has a relevant contribution to the later equilibrium charge states inside the plasma and, obviously, to the estimation of the mean charge state.

Comparing our models and estimations with experimental data from the literature, specifically, Weyrich *et al.* [31] and Hoffmann *et al.* [8], it is shown that our theoretical predictions are in good agreement with experimental results. Specifically, it is seen that the initial charge of the heavy ions is more or less zero (or minimally positive to be accelerated), which is in agreement with results presented in Ref. [31], although not those in Ref. [8]. The difference in the initial charge state between Ref. [8] and our results lies in their theoretical model to establish their initial charge because our model fits very well with the experimental data.

On the other hand, a very relevant fact is that the energy loss in plasma is higher than in the same cold gas case, confirming the well-known EPS. EPS could be due to two main effects: the increase in projectile charge state or a more efficient energy

transfer with the new free electrons created in the plasma. Focusing on the increase in the charge state is convenient comparing the energy loss of each ion with the energy loss of the proton in the same plasma conditions. Finally, it is seen that the ratio between the effective charge in plasmas and in cold gases is higher than 1 but not as high as was thought in the past.

Another relevant point is that the effective charge in plasmas Q_{eff} is greater than the mean charge state $\langle Q \rangle$. This effect is due directly to the incorporation of the BK charge distribution. When estimations are made without this distribution, they do not fit the experimental data well.

In the near future, plasmas that are more complex will be studied, such as partially ionized plasmas where the bound electrons have to be considered.

ACKNOWLEDGMENT

This work was financed by the Spanish Ministerio de Ciencia e Innovación (under Contract No. ENE2009-09276).

[1] J. Lindhard and M. Scharff, Phys. Rev. **124**, 128 (1961).
[2] L. C. Northcliffe and R. F. Schilling, At. Data Nucl. Data Tables **7**, 233 (1970).
[3] E. Nardi and Z. Zinamon, Phys. Rev. Lett. **49**, 1251 (1982).
[4] J. J. F. Ziegler, J. P. Biersack, and U. Littmark, *The Stopping and Range of Ions in Solids* (Pergamon, New York, 1985).
[5] F. Hubert, R. Bimbot, and H. Gauvin, At. Data Nucl. Data Tables **46**, 1 (1990).
[6] D. Gardes *et al.*, Europhys. Lett. **7**, 701 (1988).
[7] C. Deutsch *et al.*, Nucl. Instrum. Methods Phys. Res. A **278**, 38 (1989).
[8] D. H. H. Hoffmann, K. Weyrich, H. Wahl, D. Gardes, R. Bimbot, and C. Fleurier, Phys. Rev. A **42**, 2313 (1990).
[9] K. G. Dietrich, D. H. H. Hoffmann, E. Boggasch, J. Jacoby, H. Wahl, M. Elfers, C. R. Haas, V. P. Dubenkov, and A. A. Golubev, Phys. Rev. Lett. **69**, 3623 (1992).
[10] P. Sigmund and A. Narmann, Laser Part. Beams **13**, 281 (1995).
[11] C. Stockl *et al.*, Laser Part. Beams **14**, 561 (1996).
[12] M. Kojima, M. Mitomo, T. Sasaki, J. Hasegawa, and M. Ogawa, Laser Part. Beams **20**, 475 (2002).
[13] E. Nardi, Y. Maron, and D. H. H. Hoffmann, Laser Part. Beams **25**, 489 (2007).
[14] W. Herrmannsfeldt, J. Kwan, E. Lee, and S. Dean, Nucl. Instrum. Methods Phys. Res. A **464**, VII (2001).
[15] A. Tauschwitz, M. Demagistris, E. Boggasch, W. Laux, M. Dornik, H. Wetzler, and D. H. H. Hoffmann, IEEE Trans. Plasma Sci. **23**, 388 (1995).
[16] E. Boggasch, A. Tauschwitz, H. Wahl, K. G. Dietrich, D. H. H. Hoffmann, W. Laux, M. Stetter, and R. Tkotz, Appl. Phys. Lett. **60**, 2475 (1992).
[17] G. D. Alton, R. A. Sparrow, and R. E. Olson, Phys. Rev. A **45**, 5957 (1992).
[18] M. Chabot *et al.*, Phys. Rev. E **51**, 3504 (1995).
[19] M. Walter, C. Toepffer, and G. Zwicknagel, Nucl. Instrum. Methods Phys. Res. B **168**, 347 (2000).
[20] D. Kramer, *IEEE Particle Accelerator Conference, Albuquerque, 2007* (IEEE, New York, 2007), p. 2598.
[21] P. K. Roy *et al.*, Phys. Rev. Lett. **95**, 234801 (2005).
[22] B. Y. Sharkov, N. N. Alexeev, M. M. Basko, M. D. Churazov, D. G. Koshkarev, S. A. Medin, Y. N. Orlov, and V. M. Suslin, Nucl. Fusion **45**, S291 (2005).
[23] Y. Oguri, K. Kashiwagi, J. Kaneko, J. Hasegawa, M. Yoshida, and M. Ogawa, Phys. Rev. ST Accel. Beams **8**, 060401 (2005).
[24] D. H. H. Hoffmann *et al.*, Laser Part. Beams **23**, 47 (2005).
[25] T. Someya, T. Kikuchi, K. Miyazawa, S. Kawata, and A. I. Ogoyski, J. Phys. IV **133**, 743 (2006).
[26] B. G. Logan, R. O. Bangerter, D. A. Callahan, M. Tabak, M. Roth, L. J. Perkins, and G. Caporaso, Fusion Sci. Technol. **49**, 399 (2006).
[27] A. Bohr, Mat. Fys. Medd. K. Dan. Vidensk. Selskab **24**, 1 (1948).
[28] L. C. Northcliffe, Phys. Rev. **120**, 1744 (1960).
[29] S. Kreussler, C. Varelas, and W. Brandt, Phys. Rev. B **23**, 82 (1981).
[30] T. Peter and J. Meyertervehn, Phys. Rev. A **43**, 2015 (1991).
[31] K. Weyrich *et al.*, Nucl. Instrum. Methods Phys. Res. A **278**, 52 (1989).
[32] D. H. H. Hoffmann *et al.*, Nucl. Instrum. Methods Phys. Res. B **90**, 1 (1994).
[33] A. Golubev *et al.*, Nucl. Instrum. Methods Phys. Res. A **464**, 247 (2001).
[34] E. Nardi, D. V. Fisher, M. Roth, A. Blazevic, and D. H. H. Hoffmann, Laser Part. Beams **24**, 131 (2006).
[35] E. Fermi, Phys. Rev. **57**, 485 (1940).
[36] E. Fermi and E. Teller, Phys. Rev. **72**, 399 (1947).
[37] J. Lindhard, Mat. Fys. Medd. K. Dan. Vidensk. Selskab **28**, 1 (1954).
[38] C. Barnes and J. M. Luck, J. Phys. A **23**, 1717 (1990).
[39] N. D. Mermin, Phys. Rev. B **1**, 2362 (1970).
[40] M. D. Barriga-Carrasco and R. Garcia-Molina, Phys. Rev. A **70**, 032901 (2004).
[41] A. Selchow and K. Morawetz, Phys. Rev. E **59**, 1015 (1999).
[42] M. D. Barriga-Carrasco, Phys. Rev. E **76**, 016405 (2007).
[43] J. C. Ashley and P. M. Echenique, Phys. Rev. B **35**, 8701 (1987).
[44] I. Abril, R. Garcia-Molina, C. D. Denton, F. J. Perez-Perez, and N. R. Arista, Phys. Rev. A **58**, 357 (1998).
[45] M. Lampe, Phys. Rev. **170**, 306 (1968).
[46] E. Flowers and N. Itoh, Astrophys. J. **206**, 218 (1976).
[47] V. A. Urpin and D. G. Yakovlev, Astron. Zh. **57**, 213 (1980).
[48] J. C. Ashley and P. M. Echenique, Phys. Rev. B **31**, 4655 (1985).
[49] H. B. Nersisyan and A. K. Das, Phys. Rev. E **69**, 046404 (2004).
[50] M. D. Barriga-Carrasco, Phys. Plasmas **15**, 033103 (2008).
[51] K. Morawetz and U. Fuhrmann, Phys. Rev. E **61**, 2272 (2000).
[52] M. D. Barriga-Carrasco, Phys. Rev. E **82**, 046403 (2010).
[53] M. D. Barriga-Carrasco, Laser Part. Beams **29**, 81 (2011).
[54] C. Gouedard and C. Deutsch, J. Math. Phys. **19**, 32 (1978).
[55] N. R. Arista and W. Brandt, Phys. Rev. A **29**, 1471 (1984).
[56] W. Brandt and M. Kitagawa, Phys. Rev. B **25**, 5631 (1982).
[57] D. Gardes, A. Servajean, B. Kubica, C. Fleurier, D. Hong, C. Deutsch, and G. Maynard, Phys. Rev. A **46**, 5101 (1992).